molecular pharmaceutics

Article

Cite This: Mol. Pharmaceutics XXXX, XXX, XXX−XXX

Inhibitor−GCPII Interaction: Selective and Robust System for Targeting Cancer Cells with Structurally Diverse Nanoparticles

Jitka Neburkova,[†,‡,§] Frantisek Sedlak,[†,‡,§,∥] Jirina Zackova Suchanova,[§,∥] Libor Kostka,[⊥] Pavel Sacha,[†] Vladimir Subr,[⊥] Tomas Etrych,[⊥] Petr Simon,[†] Jitka Barinkova,[†] Robin Krystufek,[†] Hana Spanielova,[†,∥] Jitka Forstova,[∥] Jan Konvalinka,[†,#] and Petr Cigler[*,†]

[†]Institute of Organic Chemistry and Biochemistry of the CAS, Flemingovo namesti 2, 166 10 Prague, Czech Republic

[‡]First Faculty of Medicine, Charles University, Katerinska 32, 121 08 Prague, Czech Republic

[∥]Department of Genetics and Microbiology, Faculty of Science, Charles University, Vinicna 5, 128 44 Prague 2, Czech Republic

[⊥]Institute of Macromolecular Chemistry of the CAS, Heyrovskeho namesti 2, 162 06, Prague 6, Czech Republic

[#]Department of Biochemistry, Faculty of Science, Charles University, Hlavova 2030, 128 43 Prague 2, Czech Republic

Supporting Information

ABSTRACT: Glutamate carboxypeptidase II (GCPII) is a membrane protease overexpressed by prostate cancer cells and detected in the neovasculature of most solid tumors. Targeting GCPII with inhibitor-bearing nanoparticles can enable recognition, imaging, and delivery of treatments to cancer cells. Compared to methods based on antibodies and other large biomolecules, inhibitor-mediated targeting benefits from the low molecular weight of the inhibitor molecules, which are typically stable, easy-to-handle, and able to bind the enzyme with very high affinity. Although GCPII is established as a molecular target, comparing previously reported results is difficult due to the different methodological approaches used. In this work, we investigate the robustness and limitations of GCPII targeting with a diverse range of inhibitor-bearing nanoparticles (various structures, sizes, bionanointerfaces, conjugation chemistry, and surface densities of attached inhibitors). Polymer-coated nanodiamonds, virus-like particles based on bacteriophage Qβ and mouse polyomavirus, and polymeric poly(HPMA) nanoparticles with inhibitors attached by different means were synthesized and characterized. We evaluated their ability to bind GCPII and interact with cancer cells using surface plasmon resonance, inhibition assay, flow cytometry, and confocal microscopy. Regardless of the diversity of the investigated nanosystems, they all strongly interact with GCPII (most with low picomolar K_i values) and effectively target GCPII-expressing cells. The robustness of this approach was limited only by the quality of the nanoparticle bionanointerface, which must be properly designed by adding a sufficient density of hydrophilic protective polymers. We conclude that the targeting of cancer cells overexpressing GCPII is a viable approach transferable to a broad diversity of nanosystems.

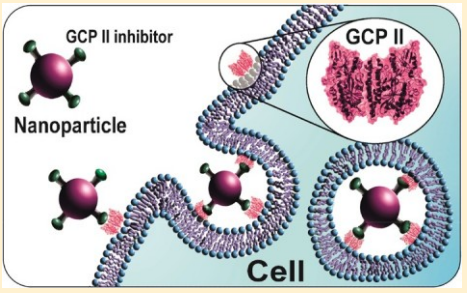

KEYWORDS: *GCPII, PSMA, inhibitor, click chemistry, targeting, cell, nanodiamond, virus-like particle, multivalent binding, polymer, nonspecific interaction*

INTRODUCTION

Targeted delivery of pharmaceuticals into tumor tissues offers promise for precise cancer diagnosis and treatment. Nanoparticle (NP)-based carriers offer several advantages over conventional therapy with cytotoxic drugs. The polyvalency of ligands strengthens binding efficacy, the size of NPs leads to prolonged blood circulation time and enables passive targeting (so-called enhanced permeation effect), and the hollow interior of NPs enables delivery of cargo.[1]

For specific cellular targeting, glutamate carboxypeptidase II (GCPII), also known as prostate-specific membrane antigen (PSMA), is a particularly interesting receptor due to its higher expression in prostate cancer tissue and cancer-associated neovasculature.[2,3] Its abundance correlates with the aggressiveness of the prostate cancer (GCPII is expressed in 80% of cells in malignant lesions[4]) and poor prognosis of the patient. In contrast to surface receptors that are present on all cell types, such as transferrin receptor, GCPII is more tissue-specific. It is primarily expressed in the prostate, central nervous system, small intestine, and kidney; expression in other tissues is much lower.[5] GCPII is a homodimeric transmembrane glycoprotein and metalloprotease with two main natural substrates, the most important of which is *N*-acetyl-L-aspartyl-L-glutamate (NAAG). In the CNS, GCPII cleaves NAAG into the neurotransmitters

Special Issue: Click Chemistry for Medicine and Biology

Received: October 10, 2017
Revised: January 22, 2018
Accepted: February 1, 2018
Published: February 1, 2018

DOI: 10.1021/acs.molpharmaceut.7b00889

N-acetyl- L-aspartate and glutamate. In the intestine, where it is also known as folate hydrolase I, GCPII participates in the cleavage of γ-linked glutamates from pteroyl-poly(γ-glutamate), freeing the vitamin folic acid.[6] Although the substrate and physiological function of GCPII in prostate remain unknown, its overexpression in prostate cancer is well-established, and the enzyme has been exploited as a highly specific target for cancer diagnostics and therapies.

Cancer cells overexpressing GCPII have been successfully targeted with NPs bearing antibodies,[7,8] nucleic acid aptamers,[9,10] and specific inhibitors.[11−14] Despite the convenient properties of small molecules, including stability, nonimmunogenicity, and ease of large-scale synthesis, using inhibitors as targeting ligands is not common. NPs bearing inhibitors have been developed for a very small number of targets, including carbonic anhydrase IX [15] and GCPII.[11−14,16−25] This may be due to the fact that enzymes localized on the plasma membrane usually are not cancer- or tissue-specific, and to the lack of known potent inhibitors for these enzymes. Nevertheless, GCPII inhibitors previously have been used with soft polymeric NPs, including in clinical trials,[19] and with inorganic NPs.[16,22,23] Because of the very different methodological approaches and NP structures used in various studies, it is difficult to compare results.

Here, we focus on exploring the structural and chemical diversity of NP systems that can be delivered to their cellular targets using interactions between small inhibitor molecules attached to the NP and GCPII on the surface of the target cell. To do so, we use representatives of different types of NPs: polymer-coated nanodiamonds, virus-like particles based on bacteriophage Qβ and mouse polyomavirus, and polymeric nanoparticles with an inhibitor attached as a targeting ligand. Although targeted nanosystems based on all these NPs have been developed previously, targeting with small molecules is typically a more challenging approach that requires surface optimization. The range of selected particles enables us to investigate nanosystems of different size, flexibility, bionanoin- terface, and conjugation chemistry. We evaluate targeting efficiency under the same conditions on the same cellular model to identify the potential limitations of these GCPII- inhibitor-targeting systems.

Nanodiamonds (NDs) are relatively polydisperse (in size and shape), nontoxic carbon NPs with unique optical properties, including near-infrared unbleachable fluorescence [derived from nitrogen vacancy (NV) centers] sensitive to magnetic and electric fields.[26] Similar to other inorganic NPs, they aggregate in electrolytes (buffers and media), driven by strong van der Waals forces.[27] NDs can be colloidally stabilized by steric hindrance, either by proteins or by polymers. Although proteins can both stabilize the particles and direct them to the intended target, electroneutral polymers also can reduce nonspecific interactions with proteins and cells, which is crucial for preparation of outstanding NPs for targeting. In a biological environment, interactions of proteins with NPs form a so-called "protein corona" on the NP surface,[28,29] which can be prevented by creating a dense polymeric shell on the NP. Intact, biocompatible, and nonimmunogenic polymers can shield the surface and minimize off-target binding.[30]

NDs without a polymer shell have been targeted to cells using the protein transferrin[31−33] or small protein toxins.[34] While use of a polymer interface can be beneficial for NPs bearing proteins, it is necessary for NPs bearing small molecules, because small molecules do not have a shielding effect on the NPs. Polymer-coated NDs bearing folic acid,[35,36] RGD peptide,[37,38] and anti-HER2 peptide[39] have been targeted to cancer cells with very high efficacy.

Virus-like particles (VLPs) are safe and noninfectious virus derived NPs, usually formed in biological systems into well-defined uniform structures by a self-assembly process from multiple copies of the same capsid protein(s). VLPs are available in various sizes and shapes and display different cell binding properties. VLPs derived from plant viruses and bacteriophages usually do not efficiently bind mammalian cells, whereas VLPs derived from mammalian viruses can bind to the mammalian cell surface, engaging the carbohydrate moieties of glycocalyx.

Mouse polyomavirus (MPyV) is an example of a small (45 nm diameter) dsDNA nonenveloped mouse virus. Historically, VLPs composed of MPyV capsid protein were the first VLPs to be used for gene transfer.[40,41] Because there is no preexisting humoral immunity to MPyV in the human population, MPyV VLPs are suitable for potential clinical use. The MPyV capsid is composed of 72 subunits. Each subunit consists of 5 molecules of the major capsid protein, VP1, which form pentamers. Under experimental conditions, guided *in vitro* disassembly and reassembly can be used for passive cargo loading into the interior of VLPs, as shown for human polyomavirus JC.[42] MPyV uses GD1a, GT1b,[43] and GT1a[44] gangliosides as primary receptors that mediate transport of the virus along an infectious pathway. Moreover, $\alpha_4\beta_1$ integrin has been identified as a secondary receptor.[45] Although viral binding to gangliosides is required for high levels of virus accumulation on the cell surface, the presence of cell-surface glycoproteins also allows for virus attachment and internalization. MPyV VLPs therefore interact with a wide variety of mammalian cells via sialic acid presented on cell surface glycoproteins and glycolipids and enter cells readily. As with NDs, surface modification of VLPs with polymers may be required for selective targeting to the specific receptor and prevention of nonspecific interactions. Recently, we demonstrated that large molecules (the protein transferrin) displayed on the MPyV surface can both retarget the VLP to cancer cells and prevent the interaction with its primary receptors.[46] Targeting with small molecules has not yet been demonstrated for MPyV VLPs.

Bacteriophage Qβ is an example of a small (28 nm diameter) icosahedral virus, VLPs of which have been actively investigated for several nanotechnology applications. Qβ VLPs are highly monodisperse and very stable, and they consist of 180 protein subunits cross-linked by disulfide linkages. Qβ VLPs can package small enzymes to protect and stabilize them.[47] Unlike other types of NPs, Qβ VLPs do not interact with mammalian cells to a great degree, and therefore they do not need to be coated with polymers to decrease nonspecific interactions and efficiently target cells. Qβ VLPs have been modified with transferrin,[48] epidermal growth factor,[49] glycan,[50] and cyclic RGD[51] to target cells, as shown by M. G. Finn and collaborators. Although a polymer coating is not needed *in vitro*, for *in vivo* applications the VLP surface should be covered with polymers to improve pharmacokinetic properties and reduce immunogenicity. Qβ particles have been modified with poly(2-oxazoline)s[52] and oligo(ethylene glycol)-methacrylate[53] to enhance thermal stability and evade immune responses.

Polymeric NPs are among the most widely used NPs for bioapplications, thanks to their variability in composition, which can be adjusted according to the needs of the application.

DOI:10.1021/acs.molpharmaceut.7b00889

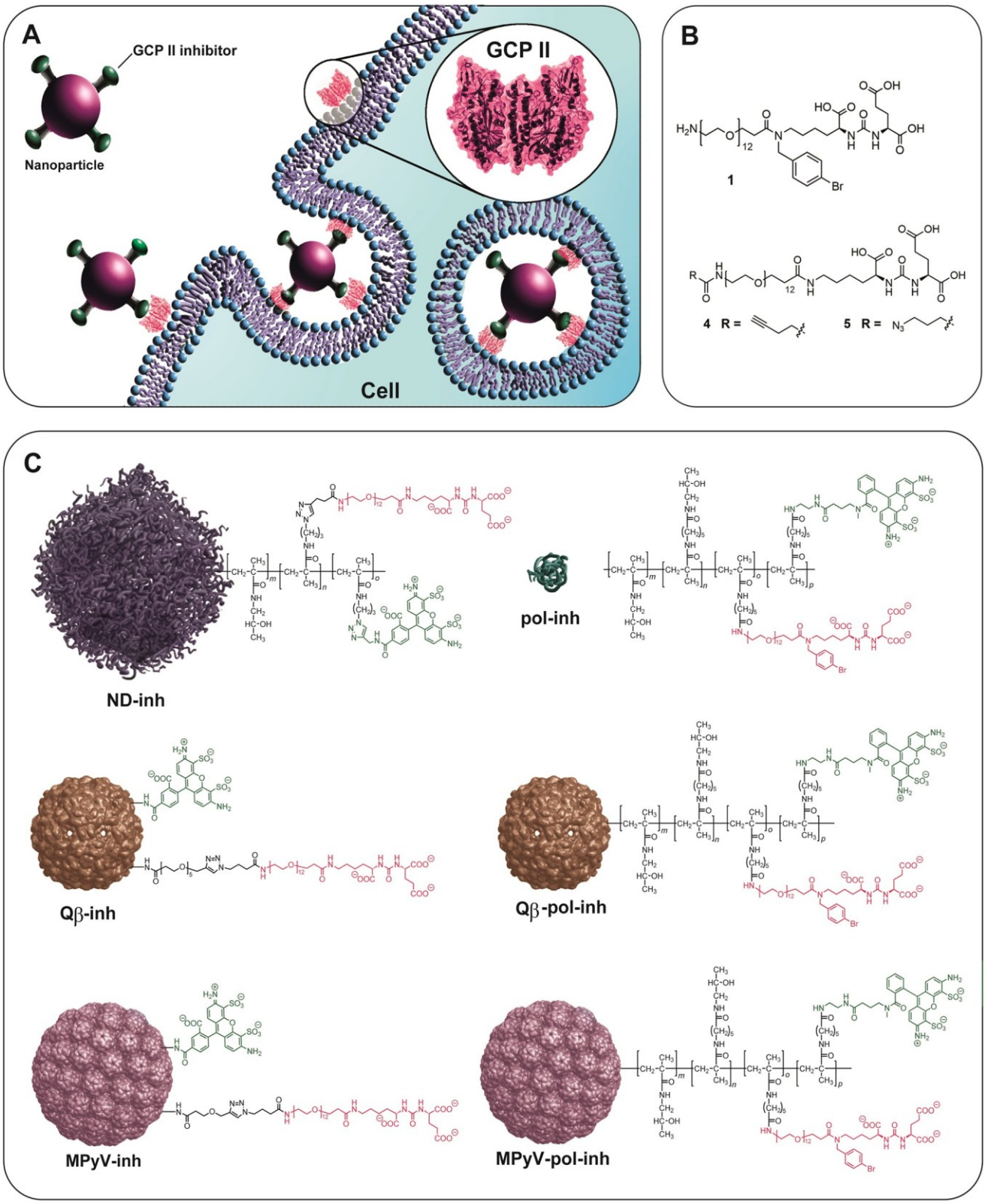

Figure 1. (A) The overall scheme of GCPII targeting using NPs bearing GCPII inhibitors. A NP bearing polyvalent array of GCPII inhibitors binds to GCPII, which is anchored in cell membrane. The nanoparticle is then endocytosed. (B) The structures of the inhibitors 1, 4, and 5 used for NP modifications. (C) Schematic illustration of the used NPs and molecular structure of their bionanointerface. Only particles modified with GCPII inhibitors are shown: nanodiamonds (ND-inh), small nanoparticles based only on the coating polymer (pol-inh), bacteriophage Qβ VLPs (Qβ-inh, Qβ-pol-inh), and mouse polyomavirus VLPs (MPyV-inh, MPyV-pol-inh). The corresponding control particles (ND, pol, Qβ, Qβ-pol, MPyV, and MPyV-pol) have always the same structure, but do not contain the GCPII inhibitors (not shown for clarity). For VLPs, the attachment of inhibitor via coating polymer is indicated by the presence of "pol" in the abbreviation, while the absence of "pol" indicates a direct attachment to surface lysines. See also Table 1 for further details.

DOI: 10.1021/acs.molpharmaceut.7b00889
Mol. Pharmaceutics XXXX, XXX, XXX−XXX

They are not prone to nonspecific interactions with cells, and therefore they are not immediately internalized. On the other hand, polymeric NPs are typically not monodisperse. Polymeric NPs are the only particles assessed in this study that have previously been used with a specific inhibitor to target GCPII. Among the most studied have been block copolymers containing a hydrophobic part, usually poly(lactid) acid, bearing the hydrophobic molecule and a hydrophilic PEG chain exposed to the environment.[12,17,19,20] For nucleic acid delivery, copolymers contained combination of polyethylenimine and PEG.[13,18] Biodegradable, nonimmunogenic, water-soluble, and biocompatible *N* -(2-hydroxypropyl)-methacrylamide (HPMA) copolymer with inhibitor targeting GCPII also has shown potential in bioapplications.[24]

The most widely used conjugation chemistry for modification of NPs with a targeting ligand is amidic coupling, which is the easiest option for molecules that naturally contain carboxyl or amine groups (such as VLPs). For amidic coupling, moieties with activated carboxyl groups with fair stability and selective reactivity to amines are needed. Here, we used the thiazolidine-2-thione group (TT) to fulfill these requirements.[54] An alternative option is use of highly effective bioorthogonal reactions, which do not have significant reactivity toward naturally occurring functional groups. The Huisgen azide−alkyne cycloaddition catalyzed by Cu(I) ions (click reaction) is popular due to its high bioconjugation efficacy without the need for protecting groups, simplicity, and variety of available substrates.[55,56] In this work, we used both amidic coupling and click reaction.

METHODS

Synthesis of GCPII inhibitors and HPMA polymers is described in the Supporting Information.

Preparation of Mouse Polyomavirus VLPs (MPyV, MPyV-inh, MPyV-PEG). MPyV particles consisting of VP1 capsid protein were produced using baculovirus expression system in *Spodoptera frugiperda* (Sf9) cells.[57] Purification of particles in cesium chloride density gradient was followed by concentration through a sucrose cushion as previously described.[57,58]

Labeling of MPyV VLPs with Alexa Fluor 488. Unmodified MPyV VLPs were dialyzed against 0.1 M HEPES, pH 7.9, and the protein concentration was adjusted to 2 mg/mL (20 mg VP1 protein in total). This solution was treated with NHS-Alexa Fluor 488 (ThermoFisher Scientific, final concentration 34 nM, 0.2 equiv per surface lysine; each MPyV VLP contains 720 surface-exposed lysines) at room temperature overnight with gentle shaking (250 rpm, TS-100C, Thermo-Shaker, Biosan). Excess dye was removed by dialysis against 0.1 M HEPES, pH 7.9 (4 °C, overnight with two buffer changes). Two-thirds of the prepared MPyV VLP mixture were used for subsequent preparation of MPyV-inh particles. The rest was purified and concentrated by centrifugation through two successive 20% sucrose cushions (35,000 rpm, SW41 Beckman rotor, 3 h) and dissolved in storage buffer (10 mM Tris-HCl, pH 7.4, 150 mM NaCl, 0.01 mM $CaCl_2$), providing the conjugate of MPyV VLPs (4 mg) used as a negative control (MPyV).

Preparation of MPyV-inh by Click Reaction. Alexa Fluor 488-labeled MPyV VLPs were first modified with the heterobifunctional linker propargyl-*N*-hydroxysuccinimidyl (NHS) ester (Sigma-Aldrich). To a solution of MPyV in 0.1 M HEPES, pH 7.9 (2 mg/mL; total amount 14 mg) was added 4.87 mg of the linker (35-fold molar excess per surface lysine) dissolved in 770 μL of DMSO (10% final concentration of DMSO). The reaction mixture was incubated at room temperature overnight with gentle shaking (250 rpm, TS-100C, Thermo-Shaker, Biosan). Excess reagents were removed by dialysis against 0.1 M HEPES, pH 7.4 (4 °C, overnight, first two buffer changes contained 10% DMSO), providing MPyV VLP−alkyne conjugate.

MPyV VLP−alkyne (5 mg in a final reaction volume of 6 mL), GCPII inhibitor 5 (see Figure 1 and Supporting Information; 213.5 nmol) in 0.1 M HEPES buffer, pH 7.4, containing 10 mM copper sulfate, 100 mM aminoguanidine, 50 mM tris(3-hydroxypropyltriazolylmethyl)amine (THPTA, synthesized according to a previously published procedure[59]), and freshly prepared 100 mM sodium ascorbate were used for click reaction. Copper sulfate and THPTA were mixed in a separate tube in a 1:5 concentration ratio prior to addition to the reaction mixture. The reaction mixture was well-sealed, mixed, and allowed to stand undisturbed at room temperature for 3 h. Excess inhibitor was removed from the resulting MPyV-inh conjugates by dialysis (cellulose ester membrane, 300 kDa, Biotech) against 0.1 M HEPES, pH 7.4 (4 °C, overnight), and storage buffer (4 °C, overnight). Finally, the MPyV-inh particles were purified and concentrated by centrifugation through two successive 20% sucrose cushions and dissolved in storage buffer.

Preparation of MPyV-PEG Particles. MPyV were dialyzed against 0.1 M HEPES, pH 8.0, with 0.01 mM $CaCl_2$ (4 °C, overnight). Then, the solution of particles (0.95 mg/mL, total amount 0.38 mg) was treated with 0.47 mg of acid-PEG_{13}-NHS ester (Broadpharm, BP-22330, 35-fold excess per surface lysine) at room temperature for 5 h on a rotating mixer. Excess reagents were removed by dialysis against TBS (20 mM Tris-HCl, 150 mM NaCl, pH 7.4) with 0.01 mM $CaCl_2$ (4 °C, overnight).

Characterization of the Particles. The quality of each preparation was examined by electron microscopy and SDS−PAGE. The amounts of VP1 were determined by Qubit protein assay kit (ThermoFisher Scientific). For matrix-assisted laser desorption/ionization mass spectrometry (MALDI) measurements, 15 μL of the sample (25 μg, 1.54 pmol) was mixed with 7.5 μL of 100 mM dithiothreitol (DTT) and 7.5 μL of 10 M urea for 10 min to disassemble the particles. According to MALDI measurements, we found 540 inhibitor molecules per MPyV-inh particle.

Preparation of Bacteriophage Qβ Particles (Qβ, Qβ-inh). Qβ particles were prepared according to a previously published procedure.[47] *Escherichia coli* BL21 (DE3) (Invitrogen) cells harboring the plasmid pET28-B (containing capsid protein) were grown in SOC supplemented with kanamycin. Starter cultures were grown overnight at 37 °C, and were used to inoculate larger cultures. Induction was performed with 1 mM IPTG at an OD_{600} of 1.0 in SOB overnight at 25 °C. Cells were harvested by centrifugation in a Beckman Coulter Avanti J-20 XP (rotor JA 17) at 5,400 rcf. The cell lysate was prepared by resuspending the cell pellet with phosphate buffer (0.1 M, pH 7.0) and sonicating at 50 W for 20 min with 5 s bursts and 5 s pause intervals. Cell debris was pelleted by centrifugation (Beckman Coulter Avanti J-20 XP) in a JA 17 rotor for 10 min (27,000 rcf), and 2 M ammonium sulfate was added to the supernatant to precipitate the Qβ VLPs. Pelleted VLPs were resuspended in phosphate buffer. Lipids and membrane proteins were then extracted from particles with 1:1 *n*-

DOI:10.1021/acs.molpharmaceut.7b00889

butanol:chloroform; Qβ VLPs remained in the aqueous layer. Crude Qβ VLPs were further purified by sucrose gradient ultracentrifugation (10−40% w:v). Particles were pelleted out from the sucrose solution by ultracentrifugation in a 70.1 Ti rotor (Beckman) at 70,000 rpm for 2 h.

Labeling of Qβ with Alexa Fluor 488. The unmodified Qβ VLPs (3 mg) were diluted in 0.1 M HEPES, pH 8 (5 mg/mL). This solution was treated with Alexa Fluor 488 5-SDP Ester (ThermoFisher Scientific, final concentration 280 μM, 0.2 equiv per surface lysine; each Qβ VLP contains 720 surface-exposed lysines) at room temperature overnight with gentle shaking (250 rpm, TS-100C, Thermo-Shaker, Biosan). Excess dye was removed by centrifugal filtration (Millipore, Amicon ultra 2 mL, cut off 100 kDa, 6 times) into 0.1 M HEPES, pH 8, providing the conjugate Qβ VLP used as a negative control (Qβ). Two-thirds of the prepared Qβ VLP mixture was used for subsequent preparation of Qβ-inh particles (Qβ-inh).

Preparation of Qβ-inh by Click Reaction. First, Qβ VLPs were modified with a heterobifunctional linker containing propargyl and NHS ester moieties (alkyne-PEG_5-NHS, Sigma-Aldrich). To a solution of Qβ VLPs in 0.1 M HEPES, pH 8 (5 mg/mL; total amount 2 mg), was added 3.94 mg of the linker (17-fold excess per surface lysine) dissolved in 40 μL of DMSO (10% final concentration of DMSO). The reaction mixture was incubated at room temperature overnight with light shaking. Excess reagents were removed by centrifugal filtration (Millipore, Amicon ultra 2 mL, cut off 100 kDa, 8 times) against 0.1 M HEPES, pH 7.4 (first two buffer changes contained 10% DMSO), providing Qβ VLP−alkyne conjugate. Qβ VLP−alkyne (1.6 mg in a final reaction volume of 160 μL), GCPII inhibitor 5 (see Figure 1 and Supporting Information; 205 nmol) in 0.1 M HEPES buffer, pH 7.4, containing 5.12 mM copper sulfate, 25.6 mM tris(3-hydroxypropyltriazolylmethyl)amine (THPTA), 40 mM aminoguanidine, and freshly prepared 40 mM sodium ascorbate were used for click reaction. Copper sulfate and THPTA were mixed in a separate tube in a 1:5 concentration ratio prior to addition to the reaction mixture. The reaction mixture was well-sealed, mixed, and allowed to stand undisturbed at room temperature for 3 h. The resulting Qβ-inh VLP conjugates were purified from excess reagents by centrifugal filtration (Millipore, Amicon ultra 2 mL, cut off 100 kDa, 8 times) into 0.1 M HEPES, pH 7.4, providing Qβ-inh conjugate.

Characterization of the Particles. The quality of each preparation was examined by electron microscopy and SDS−PAGE. The amounts of Qβ VLPs were determined by Qubit protein assay kit (ThermoFisher Scientific). For MALDI measurements, 5 μL of the sample (50 μg, 19.5 pmol) was mixed with 2.5 μL of 100 mM DTT and 2.5 μL of 10 M urea for 10 min to disassemble the particles. According to MALDI measurements, we found 180 inhibitors per Qβ-inh particle.

Preparation of Poly(HPMA)-Coated VLPs (MPyV-pol, MPyV-pol-inh, Qβ-pol, and Qβ-pol-inh). Unmodified MPyV VLPs were dialyzed and diluted to a low molarity buffer (0.67 mg/mL, 4 mM HEPES, pH 8, 20 mM NaCl, 4 μM $CaCl_2$). Unmodified Qβ VLPs (1 mg/mL) were dispersed in 25 mM HEPES buffer, pH 8. Three milliliters of MPyV particles (2 mg) was added slowly to a stirred solution of either polymer with inhibitor (pol-inh) or polymer without inhibitor (pol), both with TT reactive groups (3.76 mg/160 μL Milli-Q water, approximately 1 molar equiv to surface lysines on particles). Two milliliters of Qβ particles (2 mg) was added slowly to the stirred solution of pol-inh or pol with TT reactive groups (8.69 mg/mL Milli-Q water, approximately 0.4 equiv of surface lysines on particles). Reaction proceeded for 24 h (room temperature, mixing), and afterward remaining TT reactive groups were quenched by buffered ethanolamine (10 molar equiv to TT reactive groups). The conversion of TT reactive groups was controlled by decrease of their characteristic absorption band at 306 nm. After 12 h, no TT reactive groups were present.

VLP particles were purified by ultracentrifugation in sucrose density gradient (10−40% w:v, SW 28 Beckman rotor, 2 h 30,000 rpm for MPyV-pol and MPyV-pol-inh and 3 h 40,000 rpm for Qβ-pol and Qβ-pol-inh). Particles were pelleted out from the sucrose solution by ultracentrifugation at 35,000 rpm (SW 41Ti Beckman rotor) for 3 h.

Preparation of ND and ND-inh. NDs were pretreated and coated with a methacrylate-terminated thin silica layer, according to a previously published procedure.[60] Polymer coating was performed with slight modifications. HPMA (152 mg, 1046 μmol, purchased from Polysciences and freshly purified by FLASH chromatography) and 3-(azidopropyl)-methacrylamide (8 mg, 47.6 μmol, synthesized by methacryloylation of 3-azidopropan-1-amine with methacryloyl chloride[61]) were dissolved in DMSO (480 μL). 2,2'-Azobis(2-methylpropionitrile) (AIBN, 50 mg, 0.305 mmol, recrystallized by thickening an ethanol solution on a rotary evaporator at a maximum temperature of 30 °C) was added to the mixture. The mixture was filtered using a 0.4 μm glass microfiber microfilter. Methacrylate-terminated ND particles (8 mg, 80 μL in DMSO) were added. The reaction proceeded for 3 days under argon at 55 °C. The particles were diluted three times with methanol, centrifuged (21,000 rcf, 30 min), and purified by centrifugation with methanol (25,000 rcf, 30 min, 1 mL, 3 times). Polymer-coated NDs were further modified using azide−alkyne cycloaddition catalyzed by Cu(I) ions with Alexa Fluor 488-alkyne (purchased from Life Technologies) and GCPII inhibitor 4 (see Figure 1 and Supporting Information). NDs were modified with these two ligands in consecutive reactions utilizing the same surface functionalities. Washing procedures were employed after both modification steps. Stock solutions for copper(I)-catalyzed azide−alkyne cycloaddition reactions were prepared in water, except for the Alexa Fluor 488-alkyne, which was prepared in DMSO. The solutions of copper sulfate and THPTA were premixed (in a 1:2 concentration ratio) before they were added to the reaction mixture to yield final concentrations of 0.32 mM and 0.64 mM, respectively. The mixture was filled to the final volume with 50 mM HEPES buffer, pH 7.4. For the reaction of modified NDs with Alexa Fluor 488-alkyne, the reactants were mixed in the following order and final concentrations: colloid of poly- (HPMA)-azide modified NDs (1.2 mg in a final reaction volume of 1536 μL), Alexa Fluor 488-alkyne (10 μM), Cu-catalyst solution (see above), and a freshly prepared solution of sodium ascorbate (5 mM). The reaction mixture was well-sealed, mixed, and left for 3 h with no stirring. Modified NDs were isolated by centrifugation (20,000 rcf, 20 min) and twice washed with 1 mL of water. Half (0.6 mg) of the Alexa Fluor 488 modified NDs was reacted in a click reaction with GCPII inhibitor (320 μM) under the same conditions (in a final volume of 768 μL). Polymer-coated NDs modified with Alexa Fluor 488 (ND) and polymer-coated NDs modified with Alexa Fluor 488 and GCPII inhibitor (ND-inh) were both treated the same and were washed with water (1 mL, 7 times).

DOI:10.1021/acs.molpharmaceut.7b00889

Surface Plasmon Resonance (SPR) Measurements. All SPR measurements were performed on a four-channel SPR sensor platform (PLASMON IV) developed at the Institute of Photonics and Electronics (IPE) of the Academy of Sciences of the Czech Republic, Prague. Gold SPR chips were loaded into a pure ethanol mixture of alkanethiols containing carboxylic terminal groups [HS-$(CH_2)_{11}$-PEG_4-OH and HS-$(CH_2)_{11}$-PEG_6-O-CH_2-COOH, molar ratio 7:3, Prochimia] with a final concentration of 0.2 mM and incubated for 1 h at 37 °C. The chips were then rinsed with ethanol and deionized water, dried with flow of nitrogen, and mounted to the prism on the SPR sensor. All experiments were performed at 25 °C. The carboxyl groups present on the gold thin sensor were activated by a solution of NHS, 1-ethyl-3-[3-(dimethylamino)propyl]-carbodiimide (EDC) at final concentrations of 12.5 mM and 62.5 mM, respectively, in deionized water for 5 min at a flow rate of 20 μL/min. Excess reagents were removed at a flow rate of 30 μL/min. Next, 10 μg/mL neutravidin in 10 mM sodium acetate buffer, pH 5.0, was loaded for 6 min. Then, a high ionic strength solution (PBS with 0.5 M NaCl) was used to wash out noncovalently bound proteins, followed by 1 M ethanolamine for deactivation of residual activated carboxylic groups. Afterward, the extracellular domain of GCPII modified with biotin (Avi-GCPII, prepared according to Tykvart et al.[62]) was loaded for 10 min. Various NPs (at final concentrations of 5 nM) in TBS were injected (association phase) for several minutes, and then TBS alone was injected (dissociation phase).

Inhibition Assay. The inhibitory effects of all particles and polymers were measured as previously described with minor modifications.[63] Briefly, in each well of a 96-well plate, 250 pg of recombinant GCPII was preincubated for 5 min at 37 °C in 90 μL of reaction buffer (25 mM BisTris propane, 150 mM NaCl, 0.001% (w/w) octaethylene glycol monododecyl ester (Affymetrix), pH 7.4) with a dilution series of inhibitor (particles or polymers). The reaction was started by adding 10 μL of the substrate, 4 μM pteroyldiglutamate. The reaction was stopped after 20 min incubation at 37 °C by adding 10 μL of 25 μM 2-(phoshonomethyl)pentanedioic acid (2-PMPA) and subsequently analyzed with an Agilent 1200 series HPLC using isocratic separation in 2.7% AcCN, 19.5 mM phosphate, pH 6.0, on an Acquity UPLC HSS T3 C18 1.8 μm column (2.1 × 100 mm, Waters) with detection at 281 nm. Obtained data were fitted by logistic equation using GraphPad (GraphPad Software, Inc.), and K_i values were calculated from the log IC_{50} the using Cheng−Prusoff equation.

Flow Cytometry. Cells (U-251$^+$ MG and U-251$^-$ MG; for preparation see Supporting Information) were detached from the dish by trypsinization, resuspended in DMEM (Sigma-Aldrich D5796) supplemented with 4 mM L-glutamine (Gibco) and 10% FBS (Gibco), and counted. An appropriate amount of cells was centrifuged (300 rcf, 5 min, 4 °C) and dissolved in serum free medium without phosphate (SFM-P, DMEM, Sigma-Aldrich D3656). Subsequently, the cells were transferred into a 96-well plate (6×10^4 cells per well) and incubated with NPs (final concentration of 4 nM) for 1 h at 37 °C, 5% CO_2. This incubation was performed in triplicate and with negative controls (SFM-P only). After the treatment, cells were centrifuged (300 rcf, 5 min, 4 °C), resuspended in 200 μL of TBS, and measured with a BD LSRFortessa flow cytometry analyzer (Becton, Dickinson and Company). The data were further analyzed with BD FACSDiva Software, version 6.0. Statistical analysis was performed in R program version 3.3.1. (2016-06-21).

Confocal Microscopy. U-251$^+$ MG and U-251$^-$ MG cells (for preparation see Supporting Information) were grown in 4-chamber Glass Bottom Microwell Dishes (Cellvis, D35C4-20-1.5-N) at approximately 30% confluence, incubated for 1 h at 37 °C, 5% CO_2 with NPs, polymers (12.5 nM, diluted in SFM-P, DMEM, Sigma-Aldrich D5796), or medium only (SFM-P). Subsequently, cells were washed with TBS, fixed with 3.7% formaldehyde for 10 min, washed again in TBS, and counterstained with 500 ng/mL Hoechst 34580 solution (Thermo Scientific). Fluorescence and transmitted light (TL) images were acquired on a Zeiss LSM 780 confocal microscope with ZEN 2011 software. The images were further processed in Fiji software (contrast enhancement of Hoechst channel and TL images).[64]

RESULTS AND DISCUSSION

Design and Preparation of Nanoparticles. To inves- tigate the versatility of cell targeting using GCPII inhibitors, we prepared six different types of particles with various surface modifications, as shown schematically in Figure 1 (for clarity, we present the final investigated particles in bold, for example Qβ-inh). We attached to the surface of these NPs fluorescent labels (Alexa Fluor 488 or Atto 488; marked green in Figure 1) and GCPII inhibitors (marked red). As a targeting moiety, we used optimized urea-based inhibitors[65,63] 1, 4, and 5 that are highly polar and negatively charged, contributing to Coulombic stabilization of the particles in solution. The inhibitors were equipped by linkers terminated with either groups for click chemistry (azide, alkyne) or amino groups for conjugation to activated carboxylic acids. To remove cytotoxic Cu^{2+} ions, which can remain in the sample after click reaction, we used extensive washing procedures diluting the original concentrations of reagents by a factor of minimally 10^7 (see Methods). This decreased the copper concentration far below from cytotoxic limit, which is further suppressed by the use of THPTA ligand.[66] Furthermore, in our previous works utilizing click chemistry on similar nanoparticles,[37,46] we have observed no copper toxicity. Based on these assumptions, we have not involved cytotoxicity tests in this study.

The span of NP structural archetypes studied here includes those currently used in nanomedical applications ranging from imaging and theranostic applications to drug delivery. Polymer-coated NDs are hybrids with solid inorganic cores that retain their original shape and size during all interactions. However, their polymer shell enables flexible adjustment of targeting groups for polyvalent binding. VLPs are usually classified as soft matter nanomaterial; however, they are relatively rigid and do not undergo significant size or shape changes. Nevertheless, attachment of targeting groups to VLPs via flexible linkers can allow for a similarly flexible interaction as in polymer shells on NDs. Finally, our polymeric NPs represent the smallest and most flexible systems used in this study, and are highly susceptible to size and shape changes upon binding to a target. VLPs from both MPyV and Qβ are formed from proteins containing lysine residues with modifiable amino groups. Both types of VLPs contain approximately 720 surface lysines per particle,[50,67] which we used to modify the particles with dyes and inhibitors either by short linkages or by polymer coating. The first approach involved labeling with Alexa Fluor 488 active ester (providing negative controls and MPyV or Qβ conjugates) to allow fluorescence visualization. Then, we modified VLPs at the remaining lysines with an excess of a short linker bearing a propargyl group and attached GCPII

DOI:10.1021/acs.molpharmaceut.7b00889

inhibitor−azide conjugates via click chemistry, obtaining MPyV-inh and Qβ-inh conjugates. Because MPyV VLPs can interact with sialic acid residues, which are ubiquitously distributed and broaden MPyV cell and tissue tropism,[68] we also prepared MPyV VLPs that should avoid these interactions (MPyV-PEG). These VLPs were prepared by covering MPyV with NHS PEG_{13}-carboxyl.

The second approach for MPyV and Qβ VLP modification involved coating the VLP surface with HPMA copolymer premodified with Atto 488 dye and then with GCPII inhibitors. In addition to dye and inhibitors, the copolymers also contained hydrolytically stable TT reactive groups, which can react with lysine amino groups on the VLP surface, forming amide bonds. The reaction of VLPs with polymer proceeded overnight at pH 8. We then quenched all unreacted TT groups with ethanolamine. This step is very important because unreacted TT groups can cross-link the particles in the pellet after ultracentrifugation. We incubated the VLPs with either copolymer with inhibitor (pol-inh) or copolymer without inhibitor (pol). After purification, we obtained four different types of particles: MPyV-pol-inh, MPyV-pol, Qβ-pol-inh, and Qβ-pol (see Figure 1). The same polymer used for modification of particles was reacted in parallel with 1-aminopropan-2-ol and served as two last types of NPs (pol-inh and pol).

Coating with hydrophilic polymers greatly improves the colloidal stability of NDs in buffers and media used for bioapplications.[30] Here, we modified NDs with a thin silica layer bearing methacrylate moieties, from which polymer chains of *N*-(2-hydroxypropyl)methacrylamide and 3-(azidopropyl)-methacrylamide were grown by radical polymerization. The polymer surface enables efficient modifications, because the azide groups are randomly distributed on flexible chains without substantial steric hindrance from the surface. Using click chemistry, we equipped the NDs with GCPII inhibitor-alkyne. Although NV fluorescent centers in NDs possess excellent optical features for cell imaging,[37,69,70] for the ease of comparison with other particles in this study, we used NDs without NV centers but with attached Alexa Fluor-alkyne dye, providing ND-inh.

Characterization of nanoparticles. We characterized the size, morphology, and colloidal stability of all prepared NPs by transmission electron microscopy (TEM) and dynamic light scattering (DLS) (see Supporting Information for methods). TEM confirmed the presence of intact, highly monodispersed VLPs and fairly monodispersed ND particles (Figure 2A, Figure S1). Analysis of the particle size distribution (Figure 2B) revealed diameters of 44.7 ± 1.6 nm for MPyV-pol-inh, 27.2 ± 1.6 nm for Qβ-pol-inh, and 53.5 ± 12.0 nm for ND-inh. Using DLS, we ascertained that the particles do not aggregate (Figure 2C, Figure S2F) at 37 °C. Their hydrodynamic diameters are larger than the diameters obtained from TEM, indicating the presence of hydrated polymer shells in an aqueous environ- ment. DLS data indicated that attachment of the inhibitor through either direct conjugation or a polymer coating does not change colloidal stability of NPs.

Data obtained from SDS−PAGE analysis confirmed that unmodified VLPs can be disassembled into VP1 monomers or dimers (Figure S3). The fluorescent polymers on Qβ VLPs dissociated completely from the coat proteins during sample processing, whereas polymers on MPyV VLPs remained cross-linked with the major capsid protein VP1, forming high molecular weight complexes (Figure S3A,B). In the case of

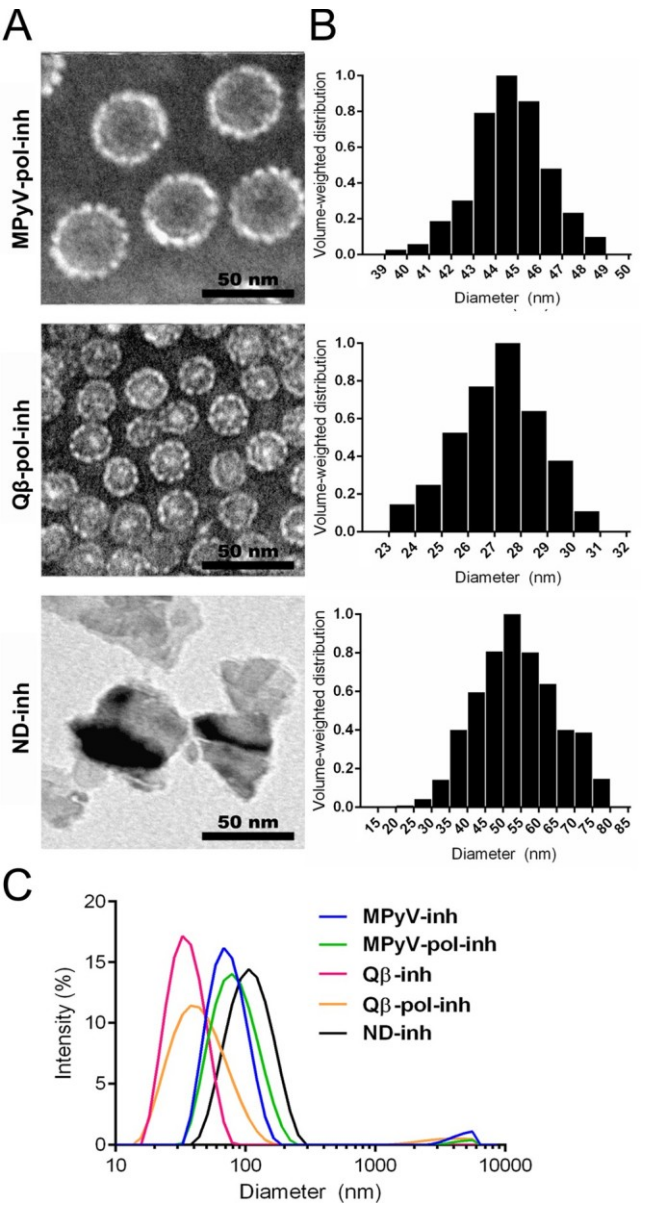

Figure 2. Characterization of NPs. (A) Representative TEM images, negative staining with 2% solution of phosphotungstic acid for MPyV-pol-inh and Qβ-pol-inh, scale bar = 50 nm. (B) Volume-weighted size distribution of the NPs according to TEM images analysis performed with ImageJ software. (C) Hydrodynamic diameters of NPs with conjugated inhibitors from DLS measurements at 37 °C (concen- tration 0.25 mg/mL in water).

directly modified VLPs (without polymers), the cross-linking phenomenon was seen in both types of VLPs, but was less pronounced in Qβ VLPs, likely resulting from different structural arrangements of particles. The absence of highly cross-linked complexes in these VLPs suggests that the particles potentially could more easily disassemble in cells to deliver cargo. NDs cannot be stained like proteins (Figure S3A); however, they were clearly detected at the start based on their fluorescent signal (Figure S3B). NDs did not migrate in the gel. Increased thermal stability of VLPs can be indicative of modification on the particle surface,[52] especially in the case of MPyV, which is structurally less stable than Qβ. We monitored temperature-induced changes in MPyV particle stability by DLS (Figure S2). Nonmodified MPyV changed size slightly at

DOI:10.1021/acs.molpharmaceut.7b00889

temperatures over 60 °C (Figure S2A), and our results corresponded well with the observed temperature midpoint of denaturation (T_M = 56 °C) for MPyV particles produced in yeast.[71] Modification with HPMA copolymer resulted in higher thermal stability (up to 80 °C) (Figure S2D,E). Particles with directly conjugated inhibitor (MPyV-inh) (Figure S2B) or PEG (negative control, MPyV-PEG) (Figure S2C) did not disassemble even after incubation at 90 °C. We assume that the increased stability of the particles is mediated by the high coverage of the MPyV surface with PEG residues, which are present in both samples (the inhibitor linker is composed of PEG). The lower stability of poly(HPMA)-coated MPyV could be caused by incomplete coverage of copolymer on the surface.

Finally, we characterized the efficiency of labeling and inhibitor loading. Due to the nonhomogeneity of dye labeling between the different types of particles, we used the relative fluorescence of particles to normalize the flow cytometry data (Table 1). From quantification of dye on poly(HPMA)-coated VLPs, we estimate that there were approximately 2 HPMA copolymers on each Qβ-pol-inh particle and 8 molecules on Qβ-pol. Surface coverage of MPyV particles (which have a larger surface area) was higher, with 30 and 35 molecules of HPMA copolymer per MPyV-pol-inh and MPyV-pol particle, respectively. In general, the number of attached HPMA copolymers was lower than we expected. We hypothesize that this may be due to the high content of TT reactive groups connected to the copolymer backbone with hydrophobic alkyl linkers. Due to the flexibility of the polymer chain, folding and formation of local hydrophobic domains can occur, leading to steric hindrance and lower reactivity of TT moieties.

Table 1. Characterization of Nanoparticle Surface Modifications, Amount of the Fluorophores on the Particles, and Relative Fluorescence Intensities of NPs[a]

particle	polymer	fluorophore	fluorophores/particle	relative fluorescence
ND	HPMA	Alexa Fluor 488	110	7.7
ND-inh	HPMA	Alexa Fluor 488	67	5.3
Qβ 488		Alexa Fluor	72	9.2
Qβ-inh 488		Alexa Fluor	44	3.9
MPyV 488		Alexa Fluor	19	4.4
MPyV-inh		Alexa Fluor 488	63	7.4
MPyV-PEG 488	PEG	Alexa Fluor	30	6.9
Qβ-pol	HPMA	Atto 488	28	12.6
Qβ-pol-inh	HPMA	Atto 488	7	4.7
MPyV-pol	HPMA	Atto 488	114	30.6
MPyV-pol-inh	HPMA	Atto 488	88	23.3
pol	HPMA	Atto 488	3	1.0
pol-inh	HPMA	Atto 488	3	1.4

[a]The fluorescence intensities of the respective NPs were measured at the same molar NP concentration. The obtained values were always normalized to the fluorescence intensity of the NP with the lowest fluorescence intensity, pol.

We also used the dye quantification data to determine the number of inhibitor molecules on polymer-coated VLPs (Table 2). Based on known stoichiometry of the dye and inhibitor in the polymer, we obtained 12 and 180 inhibitors for Qβ-pol-inh and MPyV-pol-inh, respectively. We determined the number of inhibitors on Qβ-inh and MPyV-inh by MALDI measurement after disassembling Qβ and MPyV VLPs particles to protein subunits by treatment with dithiothreitol and urea. Although the mass spectra of the modified proteins were fairly complex (Figure S4), we were able to quantify the inhibitor loads, obtaining roughly ∼180 inhibitor molecules on Qβ-inh and ∼540 on MPyV-inh (corresponding to 25 and 75% of modified surface lysines, respectively). There were approximately 1,080 PEG molecules on MPyV-PEG (determined by the same approach). MALDI measurement also confirmed that inhibitor and PEG molecules were attached to the protein covalently.

Quantification of inhibitors on ND particles was a more challenging task because they cannot be disassembled to smaller units and measured by MALDI. However, based on an analogous reaction performed under identical conditions with fluorescent dye, we can assume a load of ∼250 inhibitors per ND particle.

Interaction of NPs with GCPII *in Vitro*. To analyze interactions between NPs and GCPII molecules, we performed SPR studies and inhibition assays. SPR measurements enabled us to ascertain the capacity of NPs to bind and recognize GCPII. We immobilized GCPII on SPR chips through a neutravidin−biotin interaction (GCPII+). This connection ensures that the GCPII orientation on the gold sensor is similar to the GCPII position on the plasma membrane. As a negative control, we attached neutravidin alone (GCPII−). SPR detects changes in the refractive index in the immediate vicinity of the surface layer of a sensor chip induced by particle binding to the surface, and because the particles have different refractive indices, we cannot directly compare and quantify their binding to GCPII. However, SPR measurements of all NPs bearing inhibitor verified their selectivity and strong affinity to GCPII+ chips (Figure 3). We also observed a weak interaction between MPyV particles and GCPII− chips. This likely reflects off-target binding between VP1 protein and neutravidin, as we observed the same interaction with streptavidin (data not shown). The very low dissociation rate (k_{off}) of the NPs from GCPII indicates an extremely strong interaction between GCPII and the inhibitor attached to the NPs. We surmise that this strength is mediated by cooperative formation of multiple bonds between ligand and layer (i.e., avidity).

Next, we investigated the ability of NPs to inhibit the processing of substrate by GCPII (Table 2). Using an HPLC inhibition assay, which monitors the cleavage of the pteroyldiglutamate substrate to folate and glutamate, we measured K_i values for all NPs decorated with inhibitor as well as for free inhibitors. The small molecule inhibitors showed K_i in low nanomolar range (2−14 nM). Their attachment to nanoparticles resulted in significant increase of inhibition efficacy, reaching subnanomolar (copolymer NP) or low picomolar (other NPs) K_i values. This behavior is most likely associated with high concentration of inhibitors at the NP surface, as documented by multivalent enhancement factors[72] in range units to tens of thousands (Table 2).

In comparison with larger and more bulky targeting ligands (for example cRGD peptide[73] and transferrin,[74,75] associating with their receptors with nanomolar and low nanomolar K_d, respectively), small molecule GCPII inhibitors can be installed on nanoparticle surface conveniently at higher loadings which can result in stronger avidity effects. Correspondingly, GCPII inhibitors reach efficacy similar to small molecule folate.[76]

DOI:10.1021/acs.molpharmaceut.7b00889

Table 2. Inhibition Constants for NPs and Starting Inhibitors (for Structures, see Figure 1) Measured from HPLC Inhibition Assay, Expressed as K_i and IC_{50} with Standard Deviations[a]

	inhibitor type	inhibitors/particle	inhibition: K_i ± 1 SD [pM]	MEF	inhibition: IC_{50} ± 1 SD [pM]
			Nanoparticles		
ND-inh	4	250	3.70 ± 0.67	3780	42.1 ± 4.9
pol-inh	1	6	323 ± 50	6.63	3660 ± 290
Qβ-pol-inh	1	12	3.92 ± 0.83	546	44.6 ± 6.6
Qβ-inh	5	180	30.3 ± 4.5	373	344 ± 26
MPyV-pol-inh	1	180	2.87 ± 0.60	746	31.9 ± 4.5
MPyV-inh	5	540	0.60 ± 0.11	18 800	6.82 ± 1.2
			Inhibitors		
1			2140 ± 290		29 600 ± 4 100
4			14 000 ± 1 700		193 000 ± 26 600
5			11 300 ± 1 200		157 000 ± 19 700

[a]For NPs, the number of inhibitors per particle, inhibitor type, and multivalent enhancement factors (MEF)[72] are shown. MEF = K_i(starting inhibitor)/K_i(nanoparticle).

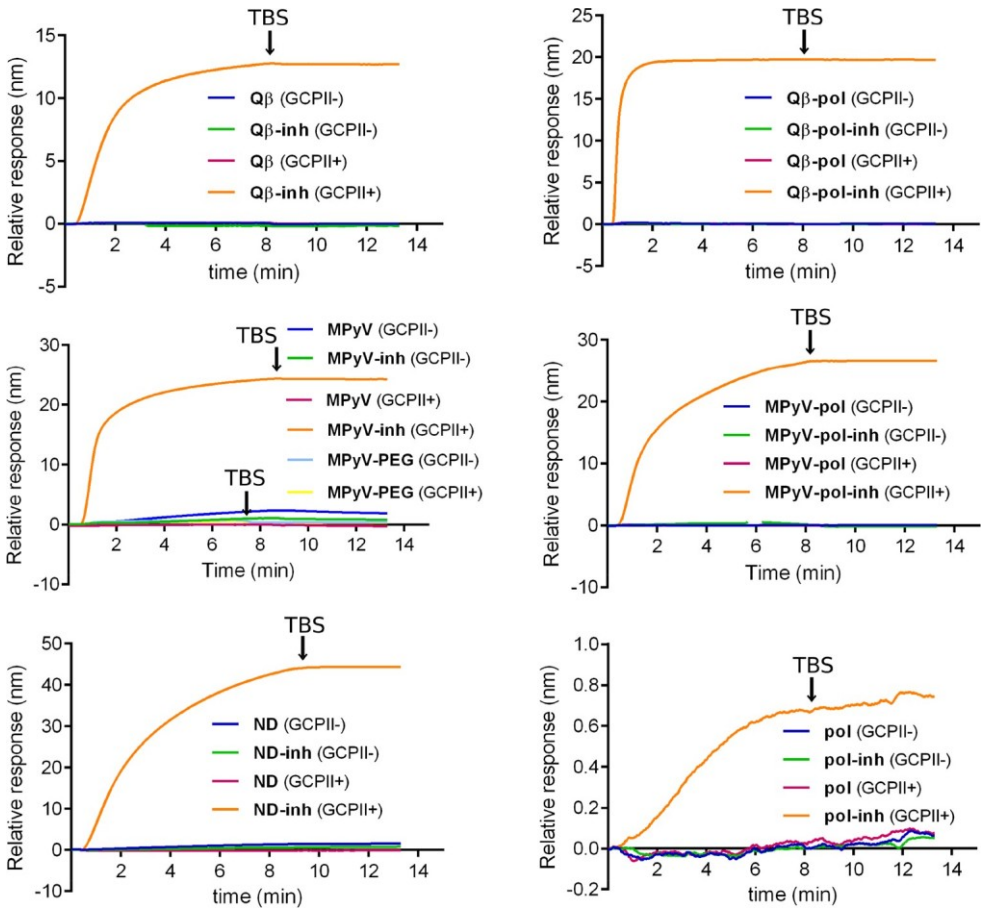

Figure 3. Interaction of NPs with GCPII. Testing of the binding capacity of all NPs to GCPII immobilized on the chip by SPR measurements. GCPII was immobilized on SPR chips through a neutravidin−biotin interaction (GCPII+). As a negative control, we attached neutravidin alone (GCPII−). NPs were injected at final 5 nM concentrations in TBS (association phase) for several minutes, and then TBS alone was injected (dissociation phase).

Cellular Uptake of NPs. Once we had verified interaction between GCPII and our modified NPs with inhibitor, we next focused on monitoring the binding ability and cellular uptake of NPs. We used the human glioblastoma cell line U-251 MG. Depending on the presence of doxycycline in the media (Tet- OffAdvanced System), these cells can overexpress GCPII on their surfaces.[63,77] This enabled us to conduct a comparative study in a very consistent way using only one type of cells. According to the level of GCPII expression, we marked the cells U-251$^+$ MG (with expression) or U-251$^-$ MG (without expression). GCPII is constantly internalized, but the turnover is greatly accelerated after binding of antibody[78,79] or HPMA copolymer with bound inhibitor.[24] The mechanism of action of polymer-induced internalization has not been studied thoroughly; however, it has been shown that antibody-induced endocytosis is clathrin-dependent and mediated by an MXXXL cytoplasmic tail motif.[79]

DOI:10.1021/acs.molpharmaceut.7b00889

We incubated all particles with cells, washed them with buffer, and analyzed the cells using flow cytometry (Figure 4, Figure S5). Because phosphate is a weak competitive inhibitor of GCPII,[80,81] we used phosphate-free buffers and media to avoid potential detachment of particles from the cell surface. Regardless of the size and loading of inhibitor, all particles with inhibitor formed strong interactions with U-251$^+$ MG cells, and relative fluorescence intensities were up to 160 times higher than those observed for U-251$^-$ MG cells (Figure 4A). With the exception of MPyV-pol-inh, the nonspecific binding of nanoparticles with inhibitor in the absence of GCPII was negligible. This is consistent with the data obtained from measurement of particles without inhibitor (Figure 4B). Consistent with previously published results, NDs,[37] polymer,[24] and Qβ particles[49] without a targeting ligand (GCPII inhibitor) did not interact with mammalian cells. In contrast, MPyV VLPs had comparably strong interactions with both U-251$^+$ MG and U-251$^-$ MG cells. We assumed that coating MPyV VLPs with polymer in MPyV-pol and MPyV-pol-inh or PEG_{13} linker (MPyV-PEG) would prevent the VP1-specific interaction with cells. Surprisingly, modification with PEG_{13} suppressed the VP1-specific binding of particles to both U-251$^+$ MG and U-251$^-$ MG cells to negligible levels, whereas MPyV-pol and MPyV-pol-inh VLPs maintained their capacity to interact with both cell variants. The higher load of PEG_{13} molecules (approximately 1,000 molecules) than poly(HPMA) molecules (approximately 30 molecules) per particle and better surface coverage indicate that an optimal load of shielding polymer is necessary to reduce the unwanted interactions of MPyV VLPs with glioblastoma cells. This is especially pronounced in our experimental system, because the U-251 MG cell line, as a representative of brain tissue derived cultures known to abundantly express complex gangliosides,[82] contains high levels of GD1a and GT1b gangliosides,[83] which are major MPyV receptors.[43,44] Interestingly, our results showed that the PEG linker itself or with the attached inhibitor molecule was capable of completely reducing VP1-mediated binding to sialic acid or selectively retargeting particles to GCPII, respectively.

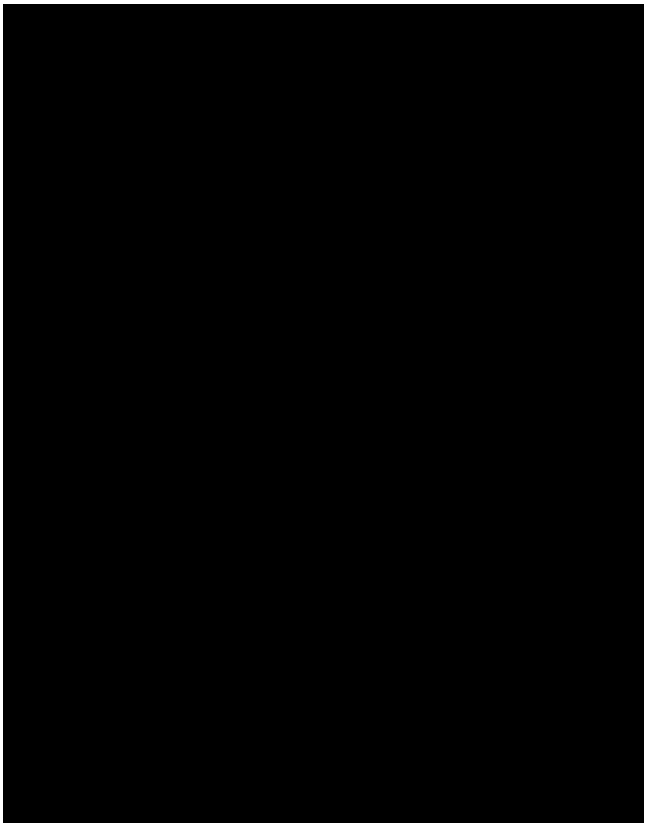

Figure 4. Flow cytometry study of NP association with U-251 MG cells with (U-251$^+$ MG) or without (U-251$^-$ MG) GCPII expression. The graphs show the interaction of NPs with (A) or without (B) inhibitor. Data represent the median of fluorescence intensity (MFI), normalized to autofluorescence of negative cells and adjusted to the relative fluorescence of particles. The standard deviations were calculated from triplicates. There were statistically significant differences between the variants containing inhibitor on U-251$^+$ MG cells and all three negative controls (NP with inhibitor on U-251$^-$ MG cells and NP without inhibitors on either U-251$^+$ MG or U-251$^-$ MG). Obtained p-values were at least $p < 0.001$, one-way ANOVA followed by Tukey's post hoc test.

We further analyzed the interaction of NPs with cells using confocal microscopy. We clearly observed a high internalization rate of NPs containing inhibitor in U-251$^+$ MG cells, and no internalization in control experiments (Figure 5A, Figure S6). MPyV VLPs were the only exception; binding of nontargeted non-PEGylated NPs was observed, similar to the flow cytometry results. We observed MPyV, MPyV-pol, and MPyV-pol-inh particles in close association with the plasma membrane (Figure 5B).

CONCLUSIONS

In summary, we investigated the robustness of GCPII targeting by a variety of NPs using one cell type model. The glioblastoma cell line U-251 MG provided us the unique possibility to switch on surface expression of GCPII using an external stimulus, instead of using different cell lines (with and without GCPII expression). We therefore were able to compare the targeting in a very consistent and straightforward way. Independent of the NP structure, size, polydispersity, used conjugation chemistry, and loading of targeting inhibitor molecules, we observed that all targeted NPs bound GCPII installed on an SPR chip, inhibited GCPII in solution, and interacted with GCPII on the cell membrane. Inhibition of GCPII was highly effective, reaching low picomolar K_i values for all particles except polymer NPs, which had subnanomolar K_i. We observed an increase in interaction efficacy of the original small molecule inhibitors upon installation on NP surface for 1 to 4 orders of magnitude. This effect is most likely caused by high local concentration of inhibitors which can lead in strong multivalent binding with the target surfaces. However, vast range of the observed enhancement documents specific needs of each nanosystem for recognition and binding.

In general, the specificity of target binding is limited not only by the strength of interaction but also by any other side interactions (either nonspecific or due to an unwanted side specificity). In the case of MPyV VLPs, the interface of which shows a broad tropism and can strongly interact with various receptors, we clearly observed the importance of the surface modification for targeting selectivity. A high load of short PEG chains grafted to surface lysines provided sufficient protection and enabled complete retargeting of MPyV VLPs to GCPII, while a low density of poly(HPMA) did not sufficiently mitigate the side binding. On the other hand, poly(HPMA) grafted from NDs at high density led to excellent and highly selective targeting.

DOI: 10.1021/acs.molpharmaceut.7b00889

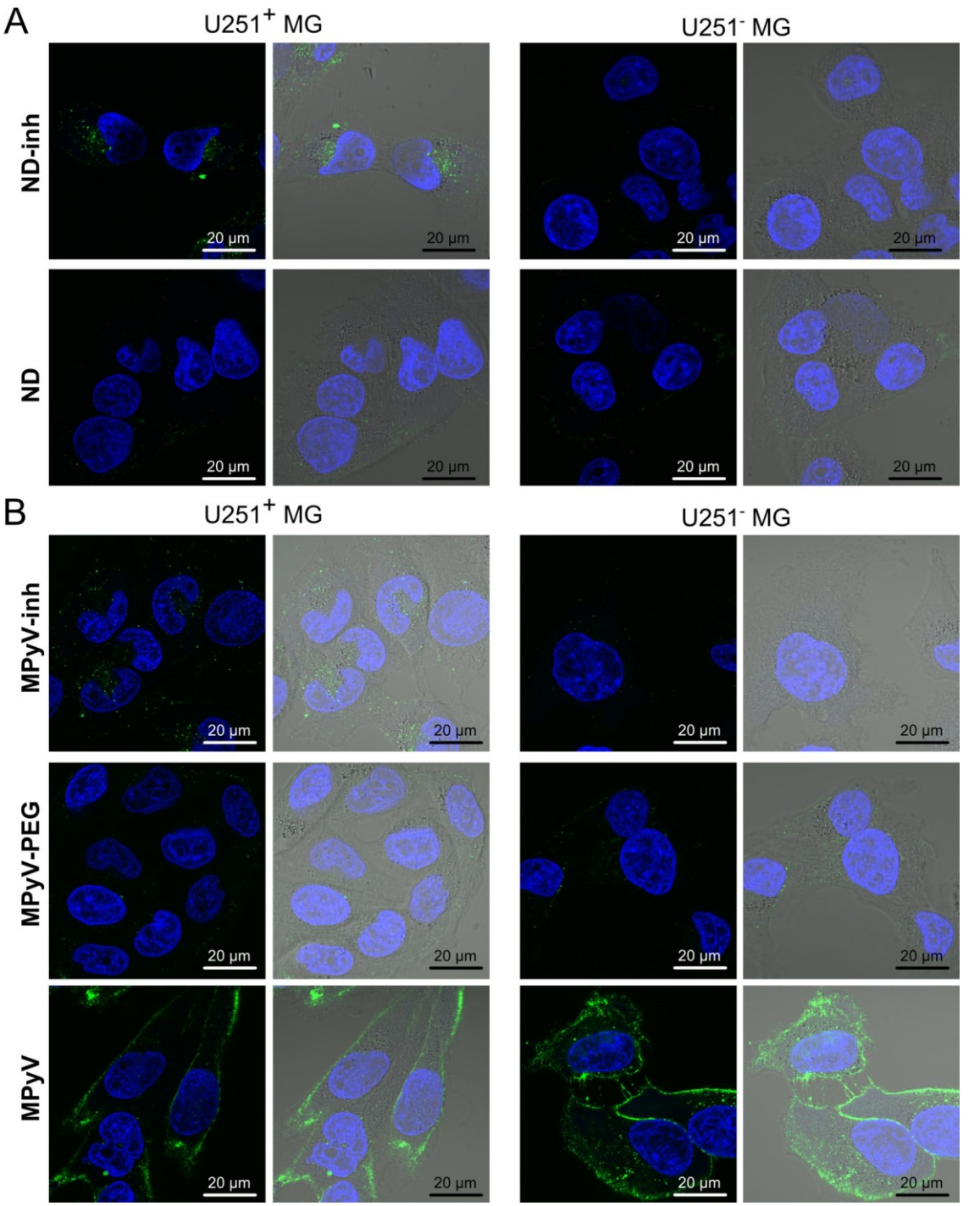

Figure 5. Confocal images of NP uptake by U-251 MG cells with (U-251$^+$ MG) or without (U-251$^-$ MG) GCPII expression incubated with NPs for 1 h. (A) Binding of ND NPs to U-251 MG cells. (B) Binding of MPyV NPs to U-251 MG cells. Confocal sections of representative cells with corresponding signal in green (NPs conjugated with Alexa Fluor 488 or Atto 488) and blue (nuclei with Hoechst staining) channels are shown. Merged images are composed of both channels and bright field image.

Our results indicate that use of small molecule inhibitors with low nanomolar range K_i displayed in polyvalent arrangements on NPs can be highly effective and selective for targeting to cells overexpressing GCPII. The robustness of the approach is limited mostly by the quality of the NP bionanointerface, which can be improved by adding a sufficient density of hydrophilic protective polymers. Based on the comprehensive data set we obtained here and on previously reported work, we believe that targeting of cancer cells overexpressing GCPII is a viable approach transferable to a broad diversity of nanosystems.

ASSOCIATED CONTENT

Supporting Information

The Supporting Information is available free of charge on the ACS Publications website at DOI: 10.1021/acs.molpharmaceut.7b00889.

Details of synthesis and characterization (PDF)

DOI:10.1021/acs.molpharmaceut.7b00889
Mol. Pharmaceutics XXXX, XXX, XXX−XXX

AUTHOR INFORMATION

Corresponding Author
*E-mail: cigler@uochb.cas.cz. Fax: (+)420-220-183-578. Tel: (+)420-220-183-429.

ORCID

Tomas Etrych: 0000-0001-5908-5182

Petr Cigler: 0000-0003-0283-647X

Author Contributions

§J.N., F.S., and J.Z.S. contributed equally.

Notes

The authors declare no competing financial interest.

ACKNOWLEDGMENTS

The authors thank Dr. Jiri Schimer for fruitful discussions and Jana Starkova for her kind help with cell culturing. This work was supported by the Grant Agency of Charles University Project No. 727816 (J.N., P.C.), Grant Agency of the Czech Republic Projects No. 16-16336S (J.N., P.C.) and 16-02938S (L.K., V.S., T.E., F.S., P.S., R.K., J.K.), League Against Cancer Prague (J.Z.S., H.S., J.F.), Project SVV-260426 (J.Z.S), Ministry of Education of the Czech Republic NPU (OP PK) InterBioMed Project LO 1302 (F.S., P.S., R.K., J.K.), and OPPK Project CZ.2.16/3.1.00/24016 (F.S., P.S., R.K., J.K.).

ABREVIATIONS USED

NP, nanoparticle; GCPII, glutamate carboxypeptidase II; PSMA, prostate-specific membrane antigen; NAAG, *N*-acetyl-L-aspartyl-L-glutamate; HPMA, *N*-(2-hydroxypropyl)-methacrylamide; ND, nanodiamond; NV, nitrogen vacancy; VLP, virus-like particle; MPyV, mouse polyomavirus; TT, thiazolidine-2-thione; Sf9, *Spodoptera frugiperda*; NHS, *N*-hydroxysuccinimide; THPTA, tris(3-hydroxypropyltriazolylmethyl)amine; DTT, dithiothreitol; SPR, surface plasmon resonance; TEM, transmission electron microscopy; DLS, dynamic light scattering; MALDI, matrix-assisted laser desorption/ionization mass spectrometry

REFERENCES

(1) Fernandez-Fernandez, A.; Manchanda, R.; McGoron, A. J. Theranostic Applications of Nanomaterials in Cancer: Drug Delivery, Image-Guided Therapy and Multifunctional Platforms. *Appl. Biochem. Biotechnol.* 2011, *165* (7−8), 1628−1651.

(2) Liu, H.; Moy, P.; Kim, S.; Xia, Y.; Rajasekaran, A.; Navarro, V.; Knudsen, B.; Bander, N. H. Monoclonal Antibodies to the Extracellular Domain of Prostate-Specific Membrane Antigen Also React with Tumor Vascular Endothelium. *Cancer Res.* 1997, *57* (17), 3629−3634.

(3) Silver, D. A.; Pellicer, I.; Fair, W. R.; Heston, W. D.; Cordon-Cardo, C. Prostate-Specific Membrane Antigen Expression in Normal and Malignant Human Tissues. *Clin. Cancer Res.* 1997, *3* (1), 81−85.

(4) Bostwick, D. G.; Iczkowski, K. A.; Amin, M. B.; Discigil, G.; Osborne, B. Malignant Lymphoma Involving the Prostate: Report of 62 Cases. *Cancer* 1998, *83* (4), 732−738.

(5) Maurer, T.; Eiber, M.; Schwaiger, M.; Gschwend, J. E. Current Use of PSMA-PET in Prostate Cancer Management. *Nat. Rev. Urol.* 2016, *13* (4), 226−235.

(6) Hlouchová, K.; Barinka, C.; Konvalinka, J. Glutamate Carboxypeptidase II as a Therapeutic Target. In *Proteinases as Drug Targets*; RSC: 2011; pp 62−95.

(7) Mukherjee, A.; Darlington, T.; Baldwin, R.; Holz, C.; Olson, S.; Kulkarni, P.; DeWeese, T. L.; Getzenberg, R. H.; Ivkov, R.; Lupold, S. E. Development and Screening of a Series of Antibody-Conjugated and Silica-Coated Iron Oxide Nanoparticles for Targeting the Prostate-Specific Membrane Antigen. *ChemMedChem* 2014, *9* (7), 1356−1360.

(8) Nagesh, P. K. B.; Johnson, N. R.; Boya, V. K. N.; Chowdhury, P.; Othman, S. F.; Khalilzad-Sharghi, V.; Hafeez, B. B.; Ganju, A.; Khan, S.; Behrman, S. W.; Zafar, N.; Chauhan, S. C.; Jaggi, M.; Yallapu, M. M. PSMA Targeted Docetaxel-Loaded Superparamagnetic Iron Oxide Nanoparticles for Prostate Cancer. *Colloids Surf., B* 2016, *144*, 8−20.

(9) Kim, D.; Jeong, Y. Y.; Jon, S. A Drug-Loaded Aptamer−Gold Nanoparticle Bioconjugate for Combined CT Imaging and Therapy of Prostate Cancer. *ACS Nano* 2010, *4* (7), 3689−3696.

(10) Kolishetti, N.; Dhar, S.; Valencia, P. M.; Lin, L. Q.; Karnik, R.; Lippard, S. J.; Langer, R.; Farokhzad, O. C. Engineering of Self-Assembled Nanoparticle Platform for Precisely Controlled Combination Drug Therapy. *Proc. Natl. Acad. Sci. U. S. A.* 2010, *107* (42), 17939−17944.

(11) Xu, X.; Wu, J.; Liu, Y.; Saw, P. E.; Tao, W.; Yu, M.; Zope, H.; Si, M.; Victorious, A.; Rasmussen, J.; Ayyash, D.; Farokhzad, O. C.; Shi, J. Multifunctional Envelope-Type siRNA Delivery Nanoparticle Platform for Prostate Cancer Therapy. *ACS Nano* 2017, *11* (3), 2618−2627.

(12) Sanna, V.; Pintus, G.; Roggio, A. M.; Punzoni, S.; Posadino, A. M.; Arca, A.; Marceddu, S.; Bandiera, P.; Uzzau, S.; Sechi, M. Targeted Biocompatible Nanoparticles for the Delivery of (−)-Epigallocatechin 3-Gallate to Prostate Cancer Cells. *J. Med. Chem.* 2011, *54* (5), 1321.

(13) Chen, Z.; Penet, M.-F.; Krishnamachary, B.; Banerjee, S. R.; Pomper, M. G.; Bhujwalla, Z. M. PSMA-Specific Theranostic Nanoplex for Combination of TRAIL Gene and 5-FC Prodrug Therapy of Prostate Cancer. *Biomaterials* 2016, *80*, 57−67.

(14) Banerjee, S. R.; Foss, C. A.; Horhota, A.; Pullambhatla, M.; McDonnell, K.; Zale, S.; Pomper, M. G. 111In- and IRDye800CW-Labeled PLA−PEG Nanoparticle for Imaging Prostate-Specific Membrane Antigen-Expressing Tissues. *Biomacromolecules* 2017, *18* (1), 201−209.

(15) Janoniene, A.; Liu, Z.; Baranauskiene, L.; Matulis, D.; Ma, M.; Salonen, J.; Hirvonen, J.; Zhang, H.; Petrikaite, V.; Santos, H. A. A Versatile Carbonic Anhydrase IX Targeting Ligand-Functionalized Porous Silicon Nanoplatform for Dual Hypoxia Cancer Therapy and Imaging. *ACS Appl. Mater. Interfaces* 2017, *9* (16), 13976−13987.

(16) Azad, B. B.; Banerjee, S. R.; Pullambhatla, M.; Lacerda, S.; Foss, C. A.; Wang, Y.; Ivkov, R.; Pomper, M. G. Evaluation of a PSMA-Targeted BNF Nanoparticle Construct. *Nanoscale* 2015, *7* (10), 4432−4442.

(17) Chandran, S. S.; Banerjee, S. R.; Mease, R. C.; Pomper, M. G.; Denmeade, S. R. Characterization of a Targeted Nanoparticle Functionalized with a Urea-Based Inhibitor of Prostate-Specific Membrane Antigen (PSMA). *Cancer Biol. Ther.* 2008, *7* (6), 974−982.

(18) Chen, Z.; Penet, M.-F.; Nimmagadda, S.; Li, C.; Banerjee, S. R.; Winnard, P. T.; Artemov, D.; Glunde, K.; Pomper, M. G.; Bhujwalla, Z. M. PSMA-Targeted Theranostic Nanoplex for Prostate Cancer Therapy. *ACS Nano* 2012, *6* (9), 7752−7762.

(19) Hoff, D. D. V.; Mita, M. M.; Ramanathan, R. K.; Weiss, G. J.; Mita, A. C.; LoRusso, P. M.; Burris, H. A.; Hart, L. L.; Low, S. C.; Parsons, D. M.; Zale, S. E.; Summa, J. M.; Youssoufian, H.; Sachdev, J. C. Phase I Study of PSMA-Targeted Docetaxel-Containing Nanoparticle BIND-014 in Patients with Advanced Solid Tumors. *Clin. Cancer Res.* 2016, *22* (13), 3157−3163.

(20) Hrkach, J.; Hoff, D. V.; Ali, M. M.; Andrianova, E.; Auer, J.; Campbell, T.; Witt, D. D.; Figa, M.; Figueiredo, M.; Horhota, A.; Low, S.; McDonnell, K.; Peeke, E.; Retnarajan, B.; Sabnis, A.; Schnipper, E.; Song, J. J.; Song, Y. H.; Summa, J.; Tompsett, D.; Troiano, G.; Hoven, T. V. G.; Wright, J.; LoRusso, P.; Kantoff, P. W.; Bander, N. H.; Sweeney, C.; Farokhzad, O. C.; Langer, R.; Zale, S. Preclinical Development and Clinical Translation of a PSMA-Targeted Docetaxel Nanoparticle with a Differentiated Pharmacological Profile. *Sci. Transl. Med.* 2012, *4* (128), 128ra39.

(21) Huang, B.; Otis, J.; Joice, M.; Kotlyar, A.; Thomas, T. P. PSMA-Targeted Stably Linked "Dendrimer-Glutamate Urea-Methotrexate" as a Prostate Cancer Therapeutic. *Biomacromolecules* 2014, *15* (3), 915−923.

DOI:10.1021/acs.molpharmaceut.7b00889

(22) Kasten, B. B.; Liu, T.; Nedrow-Byers, J. R.; Benny, P. D.; Berkman, C. E. Targeting Prostate Cancer Cells with PSMA Inhibitor-Guided Gold Nanoparticles. *Bioorg. Med. Chem. Lett.* 2013, *23* (2), 565−568.
(23) Moon, S.-H.; Yang, B. Y.; Kim, Y. J.; Hong, M. K.; Lee, Y.-S.; Lee, D. S.; Chung, J.-K.; Jeong, J. M. Development of a Complementary PET/MR Dual-Modal Imaging Probe for Targeting Prostate-Specific Membrane Antigen (PSMA). *Nanomedicine* 2016, *12* (4), 871−879.
(24) Šácha, P.; Knedlík, T.; Schimer, J.; Tykvart, J.; Parolek, J.; Navrátil, V.; Dvořáková, P.; Sedlák, F.; Ulbrich, K.; Strohalm, J.; Majer, P.; Šubr, V.; Konvalinka, J. iBodies: Modular Synthetic Antibody Mimetics Based on Hydrophilic Polymers Decorated with Functional Moieties. *Angew. Chem., Int. Ed.* 2016, *55* (7), 2356−2360.
(25) Zhu, C.; Bandekar, A.; Sempkowski, M.; Banerjee, S. R.; Pomper, M. G.; Bruchertseifer, F.; Morgenstern, A.; Sofou, S. Nanoconjugation of PSMA-Targeting Ligands Enhances Perinuclear Localization and Improves Efficacy of Delivered Alpha-Particle Emitters against Tumor Endothelial Analogues. *Mol. Cancer Ther.* 2016, *15* (1), 106−113.
(26) Rehor, I.; Slegerova, J.; Havlik, J.; Raabova, H.; Hyvl, J.; Muchova, E.; Cigler, P. Nanodiamonds: Behavior in Biological Systems and Emerging Bioapplications. In *Carbon Nanomaterials for Biomedical Applications*; Biomaterials Science and Engineering; Spring- er: Switzerland, 2016; pp 319−361.
(27) Slegerova, J.; Rehor, I.; Havlik, J.; Raabova, H.; Muchova, E.; Cigler, P. Nanodiamonds as Intracellular Probes for Imaging in Biology and Medicine. In *Intracellular Delivery II*; Prokop, A., Iwasaki, Y., Harada, A., Eds.; Springer Netherlands: Dordrecht, 2014; Vol. *7*, pp 363−401.
(28) Monopoli, M. P.; Åberg, C.; Salvati, A.; Dawson, K. A. Biomolecular Coronas Provide the Biological Identity of Nanosized Materials. *Nat. Nanotechnol.* 2012, *7* (12), 779−786.
(29) Saptarshi, S. R.; Duschl, A.; Lopata, A. L. Interaction of Nanoparticles with Proteins: Relation to Bio-Reactivity of the Nanoparticle. *J. Nanobiotechnol.* 2013, *11*, 26.
(30) Neburkova, J.; Vavra, J.; Cigler, P. Coating Nanodiamonds with Biocompatible Shells for Applications in Biology and Medicine. *Curr. Opin. Solid State Mater. Sci.* 2017, *21*, 43−53.
(31) Weng, M.-F.; Chiang, S.-Y.; Wang, N.-S.; Niu, H. Fluorescent Nanodiamonds for Specifically Targeted Bioimaging: Application to the Interaction of Transferrin with Transferrin Receptor. *Diamond Relat. Mater.* 2009, *18* (2−3), 587−591.
(32) Wang, Z.; Tian, Z.; Dong, Y.; Li, L.; Tian, L.; Li, Y.; Yang, B. Nanodiamond-Conjugated Transferrin as Chemotherapeutic Drug Delivery. *Diamond Relat. Mater.* 2015, *58*, 84−93.
(33) Li, Y.; Zhou, X. Transferrin-Coupled Fluorescence Nano-diamonds as Targeting Intracellular Transporters: An Investigation of the Uptake Mechanism. *Diamond Relat. Mater.* 2010, *19* (10), 1163−1167.
(34) Fu, Y.; An, N.; Zheng, S.; Liang, A.; Li, Y. BmK CT-Conjugated Fluorescence Nanodiamond as Potential Glioma-Targeted Imaging and Drug. *Diamond Relat. Mater.* 2012, *21*, 73−76.
(35) Chan, M. S.; Liu, L. S.; Leung, H. M.; Lo, P. K. Cancer-Cell-Specific Mitochondria-Targeted Drug Delivery by Dual-Ligand-Functionalized Nanodiamonds Circumvent Drug Resistance. *ACS Appl. Mater. Interfaces* 2017, *9* (13), 11780−11789.
(36) Zhang, B.; Li, Y.; Fang, C.-Y.; Chang, C.-C.; Chen, C.-S.; Chen, Y.-Y.; Chang, H.-C. Receptor-Mediated Cellular Uptake of Folate-Conjugated Fluorescent Nanodiamonds: A Combined Ensemble and Single-Particle Study. *Small* 2009, *5* (23), 2716−2721.
(37) Slegerova, J.; Hajek, M.; Rehor, I.; Sedlak, F.; Stursa, J.; Hruby, M.; Cigler, P. Designing the Nanobiointerface of Fluorescent Nanodiamonds: Highly Selective Targeting of Glioma Cancer Cells. *Nanoscale* 2015, *7* (2), 415−420.
(38) Zhao, L.; Xu, Y.-H.; Qin, H.; Abe, S.; Akasaka, T.; Chano, T.; Watari, F.; Kimura, T.; Komatsu, N.; Chen, X. Platinum on Nanodiamond: A Promising Prodrug Conjugated with Stealth Polyglycerol, Targeting Peptide and Acid-Responsive Antitumor Drug. *Adv. Funct. Mater.* 2014, *24* (34), 5348−5357.
(39) Zhang, T.; Cui, H.; Fang, C.-Y.; Cheng, K.; Yang, X.; Chang, H.-C.; Forrest, M. L. Targeted Nanodiamonds as Phenotype-Specific Photoacoustic Contrast Agents for Breast Cancer. *Nanomedicine* 2015, *10* (4), 573−587.
(40) Slilaty, S. N.; Aposhian, H. V. Gene Transfer by Polyoma-like Particles Assembled in a Cell-Free System. *Science* 1983, *220* (4598), 725−727.
(41) Forstová, J.; Krauzewicz, N.; Sandig, V.; Elliott, J.; Palková, Z.; Strauss, M.; Griffin, B. E. Polyoma Virus Pseudocapsids as Efficient Carriers of Heterologous DNA into Mammalian Cells. *Hum. Gene Ther.* 1995, *6* (3), 297−306.
(42) Ou, W. C.; Wang, M.; Fung, C. Y.; Tsai, R. T.; Chao, P. C.; Hseu, T. H.; Chang, D. The Major Capsid Protein, VP1, of Human JC Virus Expressed in Escherichia Coli Is Able to Self-Assemble into a Capsid-like Particle and Deliver Exogenous DNA into Human Kidney Cells. *J. Gen. Virol.* 1999, *80* (1), 39−46.
(43) Tsai, B.; Gilbert, J. M.; Stehle, T.; Lencer, W.; Benjamin, T. L.; Rapoport, T. A. Gangliosides Are Receptors for Murine Polyoma Virus and SV40. *EMBO J.* 2003, *22* (17), 4346−4355.
(44) You, J.; O'Hara, S. D.; Velupillai, P.; Castle, S.; Levery, S.; Garcea, R. L.; Benjamin, T. Ganglioside and Non-Ganglioside Mediated Host Responses to the Mouse Polyomavirus. *PLoS Pathog.* 2015, *11* (10), e1005175.
(45) Caruso, M. Role of Sialic Acid-Containing Molecules and the 4 1 Integrin Receptor in the Early Steps of Polyomavirus Infection. *J. Gen. Virol.* 2003, *84* (11), 2927−2936.
(46) Zackova Suchanova, J.; Neburkova, J.; Spanielova, H.; Forstova, J.; Cigler, P. Retargeting Polyomavirus-Like Particles to Cancer Cells by Chemical Modification of Capsid Surface. *Bioconjugate Chem.* 2017, *28* (2), 307−313.
(47) Fiedler, J. D.; Brown, S. D.; Lau, J. L.; Finn, M. G. RNA-Directed Packaging of Enzymes within Virus-like Particles. *Angew. Chem., Int. Ed.* 2010, *49* (50), 9648−9651.
(48) Banerjee, D.; Liu, A. P.; Voss, N. R.; Schmid, S. L.; Finn, M. G. Multivalent Display and Receptor-Mediated Endocytosis of Trans-ferrin on Virus-Like Particles. *ChemBioChem* 2010, *11* (9), 1273−1279.
(49) Pokorski, J. K.; Hovlid, M. L.; Finn, M. G. Cell Targeting with Hybrid Qβ Virus-Like Particles Displaying Epidermal Growth Factor. *ChemBioChem* 2011, *12* (16), 2441−2447.
(50) Rhee, J.-K.; Baksh, M.; Nycholat, C.; Paulson, J. C.; Kitagishi, H.; Finn, M. G. Glycan-Targeted Virus-like Nanoparticles for Photodynamic Therapy. *Biomacromolecules* 2012, *13* (8), 2333−2338.
(51) Hovlid, M. L.; Lau, J. L.; Breitenkamp, K.; Higginson, C. J.; Laufer, B.; Manchester, M.; Finn, M. G. Encapsidated Atom-Transfer Radical Polymerization in Qβ Virus-like Nanoparticles. *ACS Nano* 2014, *8* (8), 8003−8014.
(52) Manzenrieder, F.; Luxenhofer, R.; Retzlaff, M.; Jordan, R.; Finn, M. G. Stabilization of Virus-like Particles with Poly(2-Oxazoline)s. *Angew. Chem., Int. Ed.* 2011, *50* (11), 2601−2605.
(53) Pokorski, J. K.; Breitenkamp, K.; Liepold, L. O.; Qazi, S.; Finn, M. G. Functional Virus-Based Polymer−Protein Nanoparticles by Atom Transfer Radical Polymerization. *J. Am. Chem. Soc.* 2011, *133* (24), 9242−9245.
(54) Subr, V.; Ulbrich, K. Synthesis and Properties of New N-(2-Hydroxypropyl)methacrylamide Copolymers Containing Thiazolidine-2-Thione Reactive Groups. *React. Funct. Polym.* 2006, *66* (12), 1525−1538.
(55) Lallana, E.; Sousa-Herves, A.; Fernandez-Trillo, F.; Riguera, R.; Fernandez-Megia, E. Click Chemistry for Drug Delivery Nanosystems. *Pharm. Res.* 2012, *29* (1), 1−34.
(56) Wang, Q.; Chan, T. R.; Hilgraf, R.; Fokin, V. V.; Sharpless, K. B.; Finn, M. G. Bioconjugation by Copper(I)-Catalyzed Azide-Alkyne [3 + 2] Cycloaddition. *J. Am. Chem. Soc.* 2003, *125* (11), 3192−3193.
(57) Forstova, J.; Krauzewicz, N.; Wallace, S.; Street, A. J.; Dilworth, S. M.; Beard, S.; Griffin, B. E. Cooperation of Structural Proteins

DOI:10.1021/acs.molpharmaceut.7b00889

during Late Events in the Life Cycle of Polyomavirus. *J. Virol.* 1993, *67* (3), 1405−1413.
(58) Türler, H.; Beard, P. Simian Virus 40 and Polyoma Virus: Growth, Titration, Transformation and Purification of Viral Components. In *Virology: a practical approach*; IRL Press: Oxford, 1985; pp 169−192.
(59) Hong, V.; Presolski, S. I.; Ma, C.; Finn, M. G. Analysis and Optimization of Copper-Catalyzed Azide-Alkyne Cycloaddition for Bioconjugation. *Angew. Chem., Int. Ed.* 2009, *48* (52), 9879−9883.
(60) Rendler, T.; Neburkova, J.; Zemek, O.; Kotek, J.; Zappe, A.; Chu, Z.; Cigler, P.; Wrachtrup, J. Optical Imaging of Localized Chemical Events Using Programmable Diamond Quantum Nanosensors. *Nat. Commun.* 2017, *8*, 14701.
(61) Neburkova, J.; Hajek, M.; Rehor, I.; Schimer, J.; Sedlak, F.; Stursa, J.; Hruby, M.; Cigler, P. Targeting Glioma Cancer Cells with Fluorescent Nanodiamonds via Integrin Receptors. In *Methods in Pharmacology and Toxicology*; Humana Press: 2017; DOI: 10.1007/7653_2017_68.
(62) Tykvart, J.; Šácha, P.; Bařinka, C.; Knedlík, T.; Starková, J.; Lubkowski, J.; Konvalinka, J. Efficient and Versatile One-Step Affinity Purification of in Vivo Biotinylated Proteins: Expression, Characterization and Structure Analysis of Recombinant Human Glutamate Carboxypeptidase II. *Protein Expression Purif.* 2012, *82* (1), 106−115.
(63) Tykvart, J.; Schimer, J.; Barinková, J.; Pachl, P.; Poštová-Slavětínská, L.; Majer, P.; Konvalinka, J.; Šácha, P. Rational Design of Urea-Based Glutamate Carboxypeptidase II (GCPII) Inhibitors as Versatile Tools for Specific Drug Targeting and Delivery. *Bioorg. Med. Chem.* 2014, *22* (15), 4099−4108.
(64) Schindelin, J.; Arganda-Carreras, I.; Frise, E.; Kaynig, V.; Longair, M.; Pietzsch, T.; Preibisch, S.; Rueden, C.; Saalfeld, S.; Schmid, B.; Tinevez, J.-Y.; White, D. J.; Hartenstein, V.; Eliceiri, K.; Tomancak, P.; Cardona, A. Fiji: An Open-Source Platform for Biological-Image Analysis. *Nat. Methods* 2012, *9* (7), 676−682.
(65) Kozikowski, A. P.; Nan, F.; Conti, P.; Zhang, J.; Ramadan, E.; Bzdega, T.; Wroblewska, B.; Neale, J. H.; Pshenichkin, S.; Wroblewski, J. T. Design of Remarkably Simple, yet Potent Urea-Based Inhibitors of Glutamate Carboxypeptidase II (NAALADase). *J. Med. Chem.* 2001, *44* (3), 298−301.
(66) Hong, V.; Steinmetz, N. F.; Manchester, M.; Finn, M. G. Labeling Live Cells by Copper-Catalyzed Alkyne−Azide Click Chemistry. *Bioconjugate Chem.* 2010, *21* (10), 1912−1916.
(67) Stehle, T.; Harrison, S. C. Crystal Structures of Murine Polyomavirus in Complex with Straight-Chain and Branched-Chain Sialyloligosaccharide Receptor Fragments. *Structure* 1996, *4* (2), 183−194.
(68) Krauzewicz, N.; Cox, C.; Soeda, E.; Clark, B.; Rayner, S.; Griffin, B. E. Sustained Ex Vivo and in Vivo Transfer of a Reporter Gene Using Polyoma Virus Pseudocapsids. *Gene Ther.* 2000, *7* (13), 1094−1102.
(69) Hui, Y. Y.; Hsiao, W. W.-W.; Haziza, S.; Simonneau, M.; Treussart, F.; Chang, H.-C. Single Particle Tracking of Fluorescent Nanodiamonds in Cells and Organisms. *Curr. Opin. Solid State Mater. Sci.* 2017, *21* (1), 35−42.
(70) Wu, T.-J.; Tzeng, Y.-K.; Chang, W.-W.; Cheng, C.-A.; Kuo, Y.; Chien, C.-H.; Chang, H.-C.; Yu, J. Tracking the Engraftment and Regenerative Capabilities of Transplanted Lung Stem Cells Using Fluorescent Nanodiamonds. *Nat. Nanotechnol.* 2013, *8* (9), 682−689.
(71) Simon, C.; Klose, T.; Herbst, S.; Han, B. G.; Sinz, A.; Glaeser, R. M.; Stubbs, M. T.; Lilie, H. Disulfide Linkage and Structure of Highly Stable Yeast-Derived Virus-like Particles of Murine Polyomavirus. *J. Biol. Chem.* 2014, *289* (15), 10411−10418.
(72) Li, M.-H.; Zong, H.; Leroueil, P. R.; Choi, S. K.; Baker, J. R. Ligand Characteristics Important to Avidity Interactions of Multivalent Nanoparticles. *Bioconjugate Chem.* 2017, *28* (6), 1649−1657.
(73) Lucie, S.; Elisabeth, G.; Stéphanie, F.; Guy, S.; Amandine, H.; Corinne, A.-R.; Didier, B.; Catherine, S.; Alexeï, G.; Pascal, D.; Jean-Luc, C. Clustering and Internalization of Integrin αvβ3 With a Tetrameric RGD-Synthetic Peptide. *Mol. Ther.* 2009, *17* (5), 837−843.
(74) Fuchs, H.; Geßner, R. Iodination Significantly Influences the Binding of Human Transferrin to the Transferrin Receptor. *Biochim. Biophys. Acta, Gen. Subj.* 2002, *1570* (1), 19−26.
(75) Schüler, J.; Frank, J.; Trier, U.; Schafer-Korting, M.; Saenger, W. Interaction Kinetics of Tetramethylrhodamine Transferrin with Human Transferrin Receptor Studied by Fluorescence Correlation Spectroscopy. *Biochemistry* 1999, *38* (26), 8402−8408.
(76) Wibowo, A. S.; Singh, M.; Reeder, K. M.; Carter, J. J.; Kovach, A. R.; Meng, W.; Ratnam, M.; Zhang, F.; Dann, C. E. Structures of Human Folate Receptors Reveal Biological Trafficking States and Diversity in Folate and Antifolate Recognition. *Proc. Natl. Acad. Sci. U. S. A.* 2013, *110* (38), 15180−15188.
(77) Gossen, M.; Bujard, H. Tight Control of Gene Expression in Mammalian Cells by Tetracycline-Responsive Promoters. *Proc. Natl. Acad. Sci. U. S. A.* 1992, *89* (12), 5547−5551.
(78) Liu, H.; Rajasekaran, A. K.; Moy, P.; Xia, Y.; Kim, S.; Navarro, V.; Rahmati, R.; Bander, N. H. Constitutive and Antibody-Induced Internalization of Prostate-Specific Membrane Antigen. *Cancer Res.* 1998, *58* (18), 4055−4060.
(79) Rajasekaran, S. A.; Anilkumar, G.; Oshima, E.; Bowie, J. U.; Liu, H.; Heston, W.; Bander, N. H.; Rajasekaran, A. K. A Novel Cytoplasmic Tail MXXXL Motif Mediates the Internalization of Prostate-Specific Membrane Antigen. *Mol. Biol. Cell* 2003, *14* (12), 4835−4845.
(80) Robinson, M. B.; Blakely, R. D.; Couto, R.; Coyle, J. T. Hydrolysis of the Brain Dipeptide N-Acetyl-L-Aspartyl-L-Glutamate. Identification and Characterization of a Novel N-Acetylated Alpha-Linked Acidic Dipeptidase Activity from Rat Brain. *J. Biol. Chem.* 1987, *262* (30), 14498−14506.
(81) Barinka, C.; Rinnová, M.; Šácha, P.; Rojas, C.; Majer, P.; Slusher, B. S.; Konvalinka, J. Substrate Specificity, Inhibition and Enzymological Analysis of Recombinant Human Glutamate Carboxypeptidase II. *J. Neurochem.* 2002, *80* (3), 477−487.
(82) Schnaar, R. L.; Gerardy-Schahn, R.; Hildebrandt, H. Sialic Acids in the Brain: Gangliosides and Polysialic Acid in Nervous System Development, Stability, Disease, and Regeneration. *Physiol. Rev.* 2014, *94* (2), 461−518.
(83) Yates, A. J.; Markowitz, D. L.; Stephens, R. E.; Pearl, D. K.; Whisler, R. L. Growth Inhibition of Cultured Human Glioma Cells by Beta-Interferon Is Not Dependent on Changes in Ganglioside Composition. *J. Neuropathol. Exp. Neurol.* 1988, *47* (2), 119−127.

DOI:10.1021/acs.molpharmaceut.7b00889